Physica C: Superconductivity and its applications 532 (2017) 44–49

Contents lists available at ScienceDirect

Physica C: Superconductivity and its applications

journal homepage: www.elsevier.com/locate/physc

Localized GHz frequency electrodynamic behavior of an optimally-doped $Ba(Fe_{1-x}Co_x)_2As_2$ epitaxial film

Tamin Tai[a,b,*], Behnood G. Ghamsari[b], J.H. Kang[c], S. Lee[c], C.B. Eom[c], Steven M. Anlage[a,b]

[a] Department of Electrical and Computer Engineering, University of Maryland, College Park, Maryland 20742-3285, USA
[b] Department of Physics, Center for Nanophysics and Advanced Materials (CNAM), University of Maryland, College Park, Maryland 20742-4111, USA
[c] Department of Materials Science and Engineering, University of Wisconsin-Madison, Madison, WI 53706, USA

ARTICLE INFO

Article history:
Received 2 May 2016
Revised 22 October 2016
Accepted 30 November 2016
Available online 2 December 2016

Keywords:
Iron-Pnictide
$Ba(Fe_{1-x}Co_x)_2As_2$
Superconductivity
Microwave frequency measurement
Niobium

ABSTRACT

High frequency (several GHz) electrodynamic properties of a high-quality epitaxial, single-crystal Iron-Pnictide $Ba(Fe_{1-x}Co_x)_2As_2$ thin film near optimal doping (x = 0.08) are measured under a localized and strong RF magnetic field created by a near-field microwave microscope. Linear response and third harmonic electrodynamic measurements are performed to understand the electromagnetic properties of $Ba(Fe_{1-x}Co_x)_2As_2$ and contrasts are drawn with similar measurements on Nb. Our measurement results show that $Ba(Fe_{1-x}Co_x)_2As_2$ has nonlinear response potentially arising from a number of mechanisms and may show evidence of a multi-gap nature.

1. Introduction

The superconducting properties of iron-based superconductors have been widely discussed recently [1–3]. Because of their high critical temperature (T_c) and high upper critical field, many ideas have been proposed for potential applications in superconducting wires for high-field accelerator magnets and a variety of superconductive devices [4,5]. These applications all require a high-quality iron-based superconducting material. However it is not easy to grow a perfect single-crystal of these superconductors. The electron doped iron-pnictide $Ba(Fe_{1-x}Co_x)_2As_2$ (Ba-122 family) can be used to prepare high-quality single-crystal films by deposition of a $SrTiO_3$ (STO) or $BaTiO_3$ (BTO) template on lanthanum aluminate-strontium aluminium tantalate (LSAT) or lanthanum aluminate (LAO) perovskite substrates [6,7]. Although its application is still constrained by the requirement of a buffer layer, it appears that a large critical current density can be achieved. Questions have arisen about whether it has a single [8,9] or multiple energy gaps [3,10], without nodes [3,11,12] or with nodes [13], and whether or not it has isotropic [11,12] or anisotropic [13] gaps. This material family is still of intense interest and controversy.

Because of the success of preparing high-quality single-crystal epitaxial films of $Ba(Fe_{1-x}Co_x)_2As_2$ and of some other members of the Ba-122 family, these films are particularly suitable for the study of the iron-pnictide superconducting gap nature. From many theoretical predictions and experimental measurements, many scenarios for its gap nature are proposed and have created a great deal of debate. Some theoretical predictions have been proposed with $s^{\pm}$ symmetry of the gap on the Fermi surfaces, consistent with the ARPES measurement which shows isotropic gaps without nodes [3]. Temperature dependent penetration depth measurement with power law behavior, $\Delta\lambda(T) \propto T^n$ with $n > 2$, have been widely discussed but authors have different interpretations for the existence of either an anisotropic gap with nodes [13] or an isotropic nodeless gap [11]. Meanwhile, Raman scattering experiments indicate a gap with accidental nodes, which may be lifted by doping and/or impurity scattering in iron arsenides $Ba(Fe_{1-x}Co_x)_2As_2$ [14]. Optical measurement at terahertz frequency provides the results of either two optical gap superconductivity [10] or just one gap [9]. One reason that different, or even the same, approaches yield different results may be due to the impurity effects and surface inhomogeneities of the tested single -crystals [15]. Therefore, a localized measurement technique on these Fe-based superconductors should be applied to further illuminate the nature of the gap structure.

Scanning superconductor quantum interference device (SQUID) susceptometry has been used in localized measurement on iron pnictide superconductors to identify inhomogeneities of superconductivity, correlate these properties to the surface microstructure and to explore the gap nature [15]. This technique has been used

* Corresponding author at. Department of Electrical Engineering, University of Notre Dame, Notre Dame, Indiana 46556, USA,
E-mail addresses: ttai@nd.edu, tamintai@gmail.com (T. Tai).

http://dx.doi.org/10.1016/j.physc.2016.11.014
0921-4534/

to observe the existence of twin boundaries in the underdoped $BaFe_{1-x}Co_xAs_2$ films, along with an enhancement of the local superfluid density [16]. In addition, the relation between microstructure, grain boundaries and its critical field attracts many material science researchers to study the iron pnictide materials [17,18]. For example, the $Ba(Fe_{1-x}Co_x)_2As_2$ epitaxial films shows very high upper critical field and anisotropic physical properties due to randomly distributed $BaFeO_2$ nanorods, which yield very strong vortex pinning in the matrix of the Co-doped Ba-122 thin film [19,20].

In this study, we use our novel near field magnetic-field microwave microscope to detect the localized electromagnetic responses on $Ba(Fe_{1-x}Co_x)_2As_2$ single-crystal films with x=0.08. In contrast to scanning SQUID susceptometry, our microwave microscope [21,22] can create an intense and localized magnetic field on the scale of ~200 mT and sub-micron resolution at GHz frequencies by utilizing a hard drive magnetic write head as a scanning probe on superconductors [23–29]. This method is good for measuring harmonic generation below the superconducting transition temperature, the surface homogeneity of superconductors, and the intrinsic behavior of the superconducting order parameter. In this paper, linear response and third harmonic nonlinear response measurements on a $Ba(Fe_{1-x}Co_x)_2As_2$ film will be addressed and compared to the results on conventional Nb [26,27] superconductors. Understanding the linear and nonlinear electrodynamic response mechanisms including intrinsic and extrinsic nonlinearity in this $Ba(Fe_{1-x}Co_x)_2As_2$ film will help illuminate the nature of the iron pnictide materials.

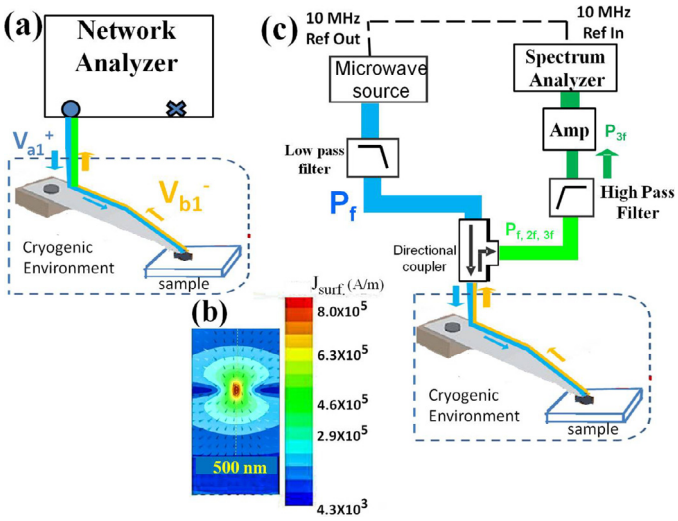

Fig. 1. (a) Schematic diagram of the linear response measurement, S_{11}, performed as a function of temperature with the network analyzer. Note that only one port (marked with a • symbol) is used in the measurement. (b) A simulated surface current density distribution (J_{surf}) on the sample surface created by the magnetic write head probe at the driving frequency is shown, assuming the probe height is 200 nm away from the sample surface [25]. (c) Schematic set up of the third harmonic measurement in nonlinear microwave microscopy. Note that the third harmonic signal (P_{3f}) is selectively filtered by the microwave circuit outside the cryogenic environment.

2. Experiment

$Ba(Fe_{1-x}Co_x)_2As_2$ with x=0.08 (thickness:200 nm) is grown by pulsed laser deposition on a (001) oriented (La,Sr)(Al,Ta)O_3 (LSAT) substrate. A 20 nm thick $BaTiO_3$ (BTO) film is deposited as a template layer before the deposition of $Ba(Fe_{1-x}Co_x)_2As_2$ films. Details of the growth conditions can be found in references [6,7]. After growth, a 20 nm thick layer of Pt is capped on the top of $Ba(Fe_{1-x}Co_x)_2As_2$ to protect the film from degradation. The resulting film has $T_c = 18.1\ K$, characterized by the temperature dependent dc resistivity $\rho(T)$ measurement.

We stimulate this $Ba(Fe_{1-x}Co_x)_2As_2$ single-crystal film locally with a strong RF magnetic field from a near-field microwave probe and then measure the reflected linear-response signal [26] and the reflected third harmonic signal. Fig. 1(a) shows a schematic diagram of the linear response measurement. A single frequency fundamental tone (V_{a1}^+) is sent out from port 1 of the network analyzer down to the probe on the $Ba(Fe_{1-x}Co_x)_2As_2$ thin film. A reflected signal (V_{b1}^-) at the same frequency is collected at the same port and then a ratioed measurement of the complex $V_{b1}^-(T)/V_{a1}^+(T)$, defined as S_{11} on the $Ba(Fe_{1-x}Co_x)_2As_2$ films, is performed at different temperatures. Note that this microscope utilizes a magnetic writer with 100 nm wide magnetic gap made by Seagate for longitudinal magnetic recording technology. The magnetic writer approaches the surface of the superconductor to a distance estimated to be on the order of 0.2 μm ~ 1 μm, which can be approximately judged by the resonant frequency perturbation of the probe assembly and by our previous measurements on many superconducting thin films, as well as High Frequency Structure Simulator (HFSS) field strength and configuration modeling. Fig. 1(b) shows the simulated HFSS result of the surface current density distribution produced by the magnetic write head probe assembly on the top of a perfect conductor [25]. The J_{surf} scale bar and arrows indicate the magnitude and direction of the screening current, respectively, in the first half of the RF cycle. In this simulation, we assume the yoke in the magnetic writer is made of ferrite. The yoke is excited by a 50 *mA* RF current and the separation between the probe and the sample is 200 nm. This creates a maximum surface current density $J_{surf} = 8 * 10^5\ A/m$.

Fig. 1(c) schematically shows the nonlinear response setup. In this case, we are gathering the localized third harmonic response generated by the superconductor. Compared to the linear response setup, the microwave circuit outside the cryogenic environment is changed to selectively filter the P_{3f} signal, and the microwave circuit inside the cryogenic environment remains the same. The fundamental principle of operation of the nonlinear microwave circuit and the response from superconductors can be found in our previous work [23,24,27].

3. Results and discussion

Localized linear responses (S_{11}) measurement is a useful tool to identify the film transition temperature T_c in a localized area and further estimate its magnetic penetration depth (λ). The black dots (connected by a solid black line) in Fig. 2 shows the temperature dependent S_{11} amplitude (Fig. 2(a)) and its phase (Fig. 2(b)) of the $Ba(Fe_{1-x}Co_x)_2As_2$ film. For comparison, a conventional Nb thin film with T_c=8.3 K is also plotted in the blue dash line. For both measurements, the incident power levels are in the linear response regime. A sharp change of amplitude and phase in S_{11} occurs near T/T_c=1 for both superconducting films, indicating the individual transition of each film. This sharp change indicates that from the normal state to the superconducting state, the surface impedance of the superconducting films suddenly changes, which results in a change of the reflected voltage (V_{b1}^-). Quantitative interpretation of this sharp change around T_c has been modeled by combining a magnetic circuit (magnetic write head inductively coupled to the sample) and transmission line (microwave circuit) [26]. However, in the $Ba(Fe_{1-x}Co_x)_2As_2$ measurement, slightly above T_c, both the amplitude and phase show a fluctuation tail before going into the normal state (compare to the Nb result). This tail most likely indicates a wider distribution of T_c values for the $Ba(Fe_{1-x}Co_x)_2As_2$ film.

The high frequency microwave nonlinear response measurement can give additional clues to figure out the electrodynamic

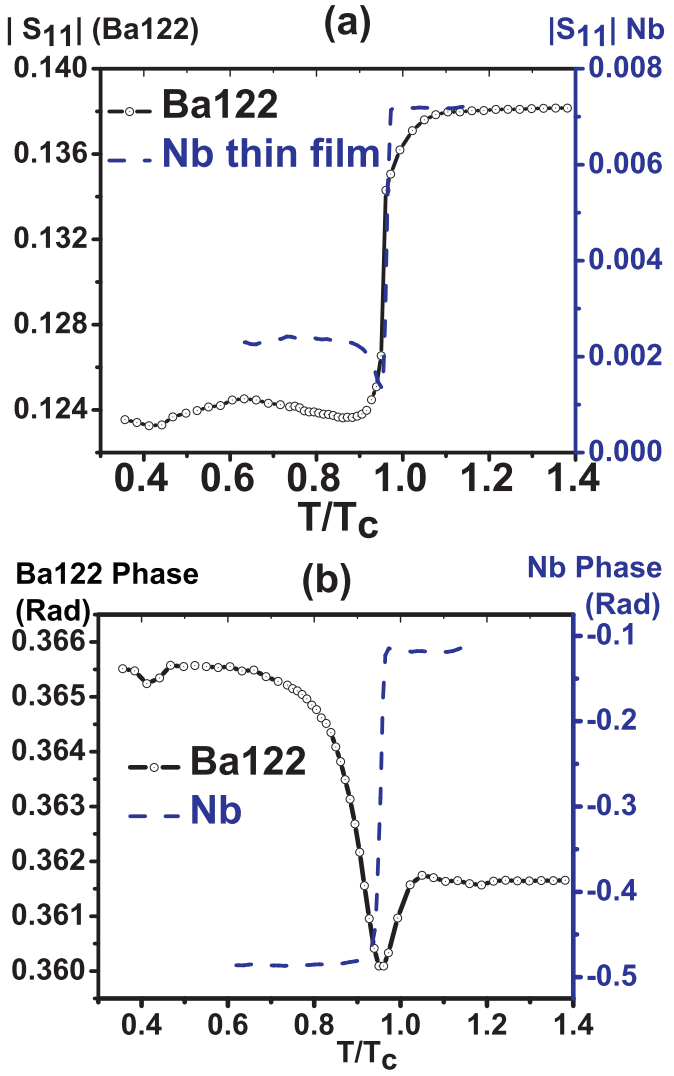

Fig. 2. The temperature dependent linear response S_{11} of the $Ba(Fe_{1-x}Co_x)_2As_2$ film measured with the near-field microwave microscope. Both (a) amplitude and (b) of S_{11} phase show a transition at normalized $T/T_c = 1$. The same measurement for (a) amplitude and (b) phase of S_{11} is also done on a Nb thin film as shown in blue dash lines for comparison. Note the T_c for the $Ba(Fe_{1-x}Co_x)_2As_2$ film and the Nb film are 18.1 K and 8.3 K, respectively. (For interpretation of the references to colour in this figure legend, the reader is referred to the web version of this article.)

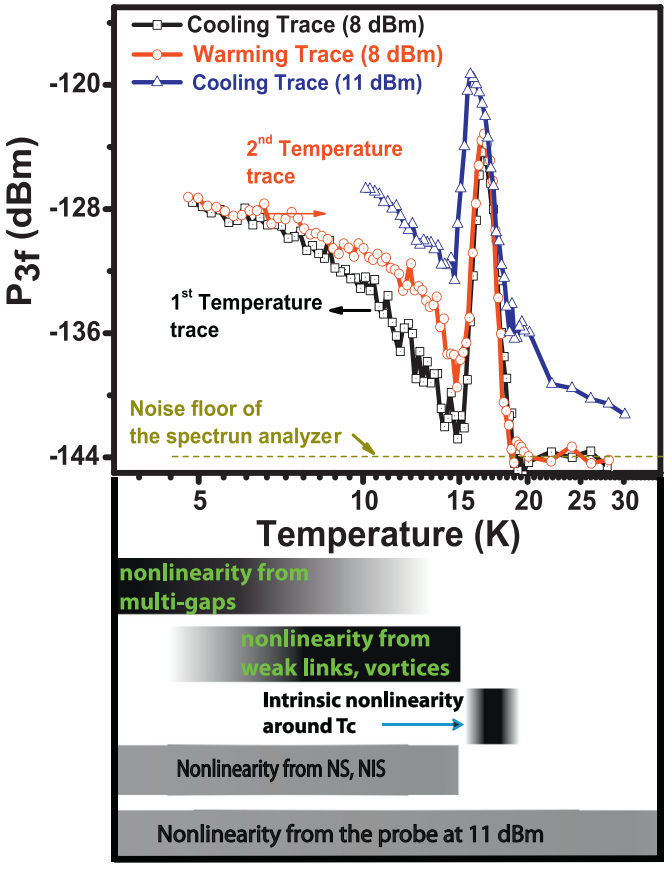

Fig. 3. Temperature dependence of the third harmonic response (log-log plot) for a 200 nm thick $Ba(Fe_{1-x}Co_x)_2As_2$ film under 5.1 GHz microwave excitation. The square and circle shapes with inner-centered dot points are experimental P_{3f} data under 8 dBm excitation. The data with blue triangular shape is taken under 11 dBm excitation. The bar plots below the figure indicate different possible nonlinear mechanisms active over different temperature regimes. (For interpretation of the references to colour in this figure legend, the reader is referred to the web version of this article.)

properties of iron-pnictide $Ba(Fe_{1-x}Co_x)_2As_2$ films. In addition, the nonlinear measurement is very sensitive to the surface defects, for example due to extrinsic defects which generate additional channels of dissipation and reactance. In order to measure the nonlinear response of this $Ba(Fe_{1-x}Co_x)_2As_2$ film, we change our microwave circuit to that in Fig. 1(c) and probe the film surface at a series of fixed positions.

Fig. 3 shows a representative result of temperature dependent third harmonic power $P_{3f}(T)$ under 5.1 GHz localized microwave excitation. Excitations at different power are performed to clarify the relation of $P_{3f}(T)$ at low (8 dBm) and high excitation power (11 dBm). The criteria of low power or high power excitation is judged by whether the probe nonlinearity is excited above the noise floor of the spectrum analyzer or not [23]. Peaks in $P_{3f}(T)$ near T_c can be interpreted as the intrinsic nonlinearity from the rf current-induced modulation of the superconducting order parameter near T_c due to the decrease of superfluid density and the associated divergence of the penetration depth [23,30,31]. Comparing the low power excitation and high power excitation $P_{3f}(T)$ curve, one finds the positions of these peaks slightly shift toward lower temperature at higher excitation power due to localized heating by microwave currents. In addition, one finds both peaks (microwave T_c) are slightly lower than the "dc zero-resistance T_c". The lower microwave T_c implies microwave measurements generally respond to lower dissipation levels, making them more sensitive than the DC resistivity measurements.

In addition, while T < 15 K, $P_{3f}(T)$ increases monotonically with decreasing temperature, a feature which is not expected from the intrinsic nonlinearity. A number of mechanisms could be responsible for this observed nonlinear response. The bottom of Fig. 3 summarizes the possibilities which we now discuss in detail.

This observed temperature dependence of $P_{3f}(T)$ is reminiscent of that arising from Josephson weak links [32] or Josephson vortices in a large Josephson junction in YBCO [33] and $Ba(Fe_{1-x}Co_x)_2As_2$. From 15 K to 6 K at 8 dBm excitation, one can find the cooling down nonlinear trace and warming up nonlinear re-trace shows a hysteretic behavior [34]. This implies that extrinsic nonlinearity due to oscillation and motion of trapped vortices [35] in the grain boundaries of the film would be one of the possible nonlinear mechanisms at this intermediate temperature regime.

Because the thickness of this film is always smaller than the penetration depth, the magnetic flux coming out from the magnetic gap of the writer probe could go through the film, which not only results in the Josephson vortices in the grain boundaries of the film but also form a vortex and antivortex pair perpendicular to the film. This situation is analogous to having a parallel mag-

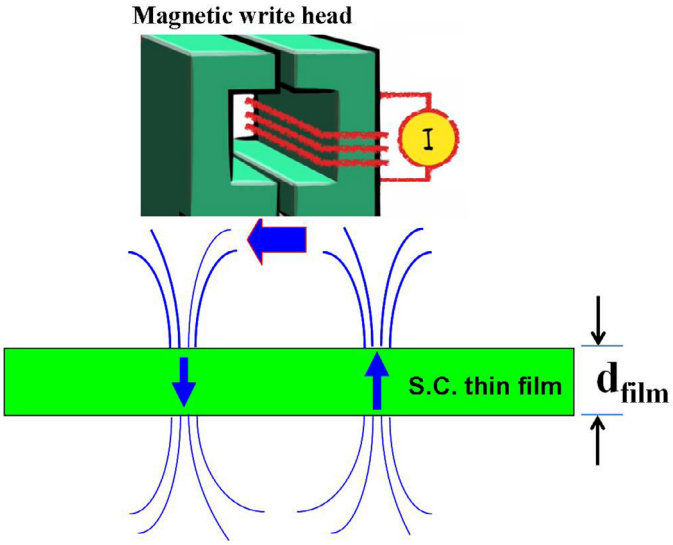

Fig. 4. Schematic illustration of the magnetic flux coming from the yoke of the magnetic write head to the superconducting thin film. This situation is analogous to a magnetic dipole on top of the superconducting thin film (horizontal blue arrow). A vortex and antivortex perpendicular to the film tend to form if the film thickness $d_{film} \ll \lambda$. Figure not to scale. (For interpretation of the references to colour in this figure legend, the reader is referred to the web version of this article.)

netic dipole on top of the superconducting thin film (horizontal blue arrow in Fig. 4). A vortex and an antivortex nucleate perpendicular to the film and will move under the influence of the RF screening currents in the film. One can model this situation with an equivalent point magnetic dipole that is horizontally-oriented and placed above the superconducting thin film. Once the vortices are inside the film, pinning can occur by the randomly distributed $BaFeO_2$ nanorods in the matrix of the Co-doped Ba-122 thin film. The pinned vortices will oscillate under the influence of the fundamental RF currents and generate harmonic response [34,36–38]. Hence the creation, motion and pinning of perpendicular vortex and antivortex pairs will generate high order harmonic response in the intermediate temperature region, consistent with our data.

At temperatures T < 6 K at 8 dBm excitation power shown in Fig. 3, there is no hysteresis behavior. This implies that extrinsic nonlinearity due to vortices does not dominate the nonlinear response because of the increase of pinning force due to the increase of critical current at lower temperature. In addition, the probe nonlinearity, P_{3f}^{probe} at 8 dBm is under the noise floor of the spectrum analyzer, and would not affect the measured P_{3f} (which will be discussed in Fig. 5). One possibility is nonlinearity due to Josephson coupling between multiple superconducting gaps in $Ba(Fe_{1-x}Co_x)_2As_2$. This mechanism will be discussed in more detail with the power-dependent nonlinear response data presented below.

Another possibility is the nonlinearity coming from transport through normal metal-superconducting (NS) junctions [39]. Note that the $Ba(Fe_{1-x}Co_x)_2As_2$ film is capped with a 20 nm thick Pt layer. Therefore an NS interface will produce proximity-induced subgap states which are probed by the RF field. In addition, if the interface of the NS junction has impurities or vacancy defects, the normal metal-insulator-superconducting (NIS) junctions may also be formed. Then localized surface states due to the NIS junctions in the multi-band superconductor can also produce significant nonlinearity even in the absence of nodes. We are not aware of quantitative analysis of temperature dependent nonlinearity from NS and NIS junctions in the Ba-122 family.

One of the approaches to understand the intermediate and low temperature nonlinear mechanisms is measurement of the dependence of nonlinearity on the fundamental tone power. Fig. 5(a) shows the dependence of P_{3f} on P_f at a fixed position and some selected temperatures for this 200 nm thick $Ba(Fe_{1-x}Co_x)_2As_2$ film. In the normal state (T > 18.1 K), the measured nonlinearity comes from the probe itself because the magnetic write head is made of ferrite which generates background nonlinearity [23]. Note that the probe third harmonic response (P_{3f}^{probe}), which also depends on the probe height, only becomes measurable at high excitation powers (above 10 dBm). For measurement below T_c, all curves (at temperature T_1, T_2 and T_3) show a sharp P_{3f} onset from the noise floor of the spectrum analyzer. After the onset, the nonlinearity continues to increase with fundamental power until a turnover point. After the turnover point, the nonlinearity goes down until it approaches the curve of probe nonlinearity, P_{3f}^{probe} (data taken at $T = T_N$). After that point, the measured nonlinearity oscillates around the curve of probe nonlinearity as the two contributions interfere constructively and destructively. Fig. 5(b) is the same type of power dependent measurement of P_{3f} on P_f but on a bulk Nb superconductor

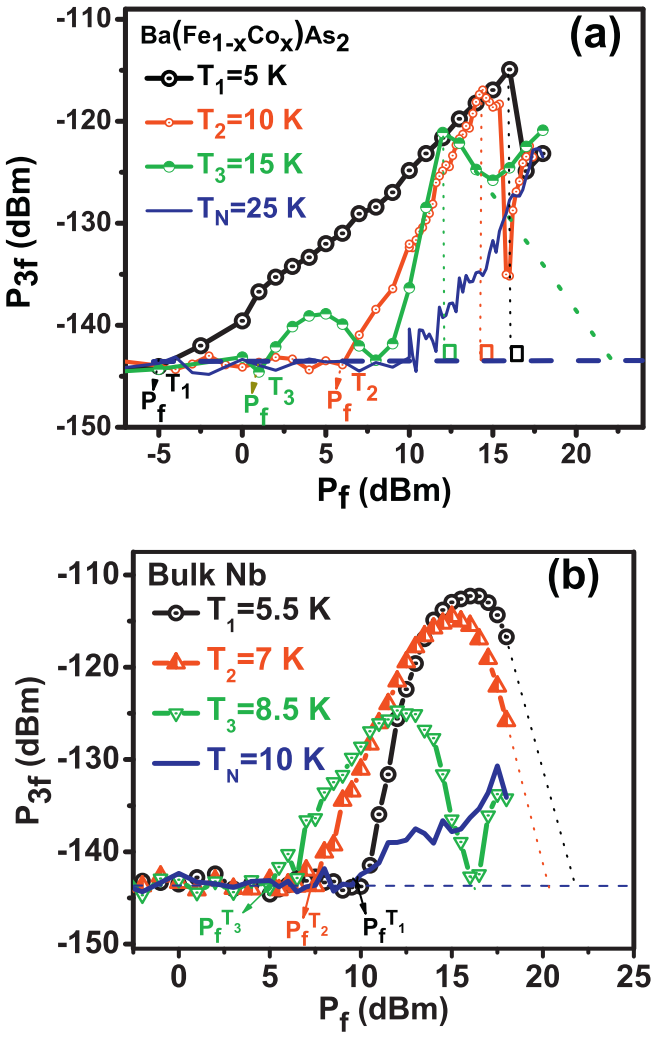

Fig. 5. (a) Dependence of P_{3f} on P_f for a 200 nm thick $Ba(Fe_{1-x}Co_x)_2As_2$ film under 5.1 GHz local microwave excitation. The vertical dashed lines for $T_1 = 5$ K and $T_2 = 10$ K indicate the turnover point. Another dashed line on the T_3=15 K curve indicates the extrapolation of P_{3f} on P_f through the probe nonlinearity, P_{3f}^{probe}, which is taken at T_N=25 K above the T_c of the $Ba(Fe_{1-x}Co_x)_2As_2$ film. The horizontal dashed line indicates the noise floor (~ -143 dBm) of the spectrum analyzer. (b) Power dependence of P_{3f} on P_f for a bulk Nb sample under 5.36 GHz local microwave excitation [27]. The dashed line in each curve indicates the extrapolation of P_{3f} on P_f through the P_{3f}^{probe} to the noise floor of the spectrum analyzer. The T_c of this bulk Nb is 9.2 K and P_{3f}^{probe} is taken at T_N=10 K.

for comparison. All curves also have a sharp P_{3f} onset from the noise floor of the spectrum analyzer, which is −142.5 dBm in this measurement. Nonlinearity keeps growing before a turnover point and then drops gradually to follow the probe nonlinearity. Each curve in Fig. 5(a) and (b) looks qualitatively similar but there are many differences upon closer examination.

First, the relation of temperature dependent onset is different. In the bulk Nb measurement, the relation of onset power for each temperature is $P_f^{T_3} < P_f^{T_2} < P_f^{T_1}$. Therefore for conventional superconductors such as Nb, the onset of nonlinearity requires higher excitation power at lower temperatures because the sample remains in the Meissner state and because of the larger critical field ($\sim H_{c1}$) at lower temperature. However, in the $Ba(Fe_{1-x}Co_x)_2As_2$ measurement, one can clearly see the relation of onset power is the opposite, $P_f^{T_2} > P_f^{T_1}$ and $P_f^{T_3} > P_f^{T_1}$. This means nonlinearity can be easily excited at lower temperature (T=5 K). One interpretation of this low-temperature nonlinear response is that it is due to an intrinsic nonlinearity arising from Josephson coupling between two or more gaps in the $Ba(Fe_{1-x}Co_x)_2As_2$ film (mentioned briefly in the discussion of Fig. 3). Hence, the variable phase difference of the coupled superconducting gaps will produce the nonlinear response when a nonequilibrium charge imbalance appears at short length scales [40], essentially the nonlinear mechanism associated with excitation of the Leggett mode for two gap superconductors [40]. Note that the situation of charge imbalance can be easily created from the perpendicular component of the RF magnetic field as shown in Fig. 4.

Secondly, after a little increase of P_f from the point of turnover on each P_{3f} versus P_f curve, one can see a sharp drop at T=5 K and T=10 K in Fig. 5(a). These sharp drops are not observed in Nb, and suggest the sudden loss of a nonlinearity mechanism. For example it could be the annihilation of a superconducting order parameter in high RF magnetic field, implying that perhaps one of the superconducting gaps is suddenly destroyed by localized intense magnetic field on the $Ba(Fe_{1-x}Co_x)_2As_2$ film surface. At that point, the Leggett mode nonlinearity is eliminated due to the loss of the second gap, reducing the P_{3f} output suddenly.

In addition, for $Ba(Fe_{1-x}Co_x)_2As_2$ films as shown in Fig. 5(a), the shape of P_{3f} on P_f at T=15 K is different from that at T=5 K and 10 K. At T=15 K, there is no sharp drop after the turnover point. This shape is similar to that measured from bulk Nb at all temperatures. This implies that at T=15 K, nonlinearity comes from an extrinsic nonlinear response, as seen in bulk Nb. This specific curve shape is very similar to that predicted for entry and exit of vortices in Josephson coupled rings [27,43], which indicates the nonlinearity at T=15 K comes from the dynamics of vortex penetration, jumpwise instabilities in the $Ba(Fe_{1-x}Co_x)_2As_2$ film under strong and localized RF fields. This is consistent with the hysteretic behavior seen in Fig. 3. An extrapolation dashed line in Fig. 5(a) similar to the plot on Nb may indicate the presence of another superconducting gap (large gap) of $Ba(Fe_{1-x}Co_x)_2As_2$ at this temperature. Hence the co-existence of a sharp drop of P_{3f} on P_f and extrapolation plot to indicate the annihilation of superconducting gaps on the P_{3f} versus P_f curves is consistent with a multigap nature of $Ba(Fe_{1-x}Co_x)_2As_2$.

Finally, the excitation level of these turnover points at each temperature should be proportional to the temperature dependent lower critical field of the smallest energy gap of $Ba(Fe_{1-x}Co_x)_2As_2$. Fig. 6 shows a summary plot of the estimated surface B field at the turnover peak points (B_{turn}) versus the corresponding temperature. The corresponding P_{3f} at the turnover point is also plotted and indicated as Max(P_{3f}) on a linear power scale in Watts. The surface RF magnetic field is converted from P_f by the relation of $P_f(T) = k[B_{turn}(T)]^2$, where k a constant relating the incident power in the probe to the RF magnetic field experienced by the sample surface, and $k = 25.6W/T^2$ is taken [27]. This number is judged by the field scale generated by HFSS simulation in Fig. 1(b) and experimental results on a known Nb conventional superconductor for calibration. One can find the temperature dependent surface B field at the turnover peak points is similar to the temperature dependent critical field. A fit of temperature dependent B_{turn} is done by tuning the value of T_c', n and B_0 of the following approximation equation:

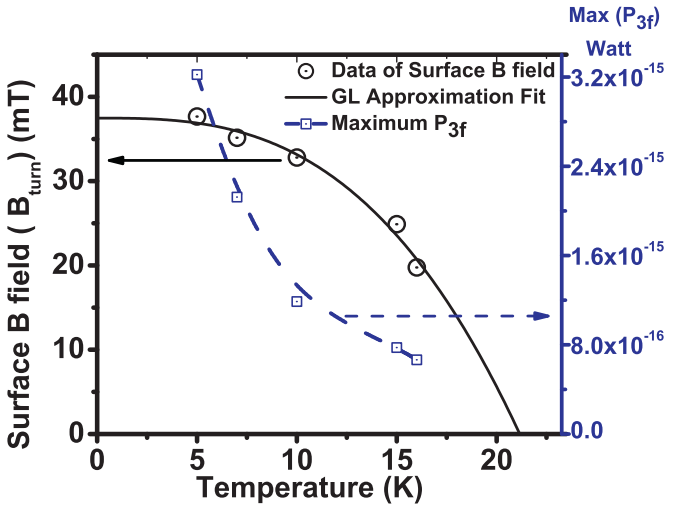

Fig. 6. Temperature dependent estimated surface critical magnetic field (B_{turn}) of $Ba(Fe_{1-x}Co_x)_2As_2$ and corresponding P_{3f} (indicated as Max(P_{3f})) in Watts at the turnover point. Note that the dashed line is a B-Spline fit. The solid line is a fit of the surface critical magnetic field from Eq. (1). with $T_c' = 21.15$ K, $n = 2.88$ and $B_0 = 37.47$ mT.

$$B_{turn}(T) = B_0\left(1 - \left(\frac{T}{T_c'}\right)^n\right) \tag{1}$$

With $T_c' = 21.15$ K, $n = 2.88$ and $B_0 = 37.47$ mT, one can get the smallest standard deviation between experimental data points and the approximation equation as shown on the plot of the solid line in Fig. 6. The B_0 perhaps can be interpreted as the lower critical field B_{c1} for fields along the c-axis of the Ba-122 film. Given an upper critical field $B_{c2}(T = 0\ K) \sim 100\ T$ and Ginzburg–Landau (GL) parameter $\kappa = \lambda/\xi_{GL} \sim 10^2$ [2,41], where ξ_{GL} is the superconducting coherence length, one can predict that the value of B_{c1} for Ba-122 single-crystal is on the order of 25 mT [2]. The B_0 from the fitting is also very close to the experimentally measured lower critical field on another iron-pnictide superconductor $BaFe_2(As_{1-x}P_x)_2$ with $B_{c1}(T = 0\ K) = 30$ mT ~ 60 mT for different Phosphorus doping [42]. Measurement of the dependence of P_{3f} on P_f at different positions shows ±2.5 dB variations of B_{turn} at the same temperature. This may be due to lateral variations in this epitaxial thin film or slightly different probe height.

4. Summary

From the temperature dependent linear responses measurement, the $Ba(Fe_{1-x}Co_x)_2As_2$ film shows a relatively wide superconducting transition width at its T_c. From the temperature dependent $P_{3f}(T)$ measured at 8 dBm excitation power, different nonlinear mechanisms in different temperature regions are seen. At temperatures around T_c, the nonlinearity comes from the current-induced modulation of the suppressed superconducting order parameter near T_c. In the intermediate temperature range, nonlinearity is dominated by the motion of vortices. At temperatures below 6 K, the possibility of NS junction nonlinearity or multi-gap nonlinearity may be present. The third harmonic power (P_{3f}) de-

pendence on fundamental tone power (P_f) shows that nonlinearity at low temperature can be easily stimulated at very low excitation power, quite different from the results on Nb, a conventional single gap s-wave superconductor. Therefore, from the localized high field electrodynamic measurements, the $Ba(Fe_{1-x}Co_x)_2As_2$ superconductor shows behavior consistent with a multigap nature.

Acknowledgement

This work is supported by the US Department of Energy / High Energy Physics through grant # DE-SC0012036T and CNAM. Research at UW-Madison (Design and synthesis of thin film heterostructures used in this work) was supported by the US Department of Energy, Office of Basic Energy Sciences, Division of Materials Sciences and Engineering under award number DE-FG02-06ER46327 (C.B.E.).

References

[1] J. Paglione, R.L. Greene, High-temperature superconductivity in iron-based materials, Nat. Phys. 6 (2010) 645.
[2] A. Gurevich, Iron-based superconductors at high magnetic fields, Rep. Prog. Phys. 74 (2011) 124501.
[3] K. Terashima, Y. Sekiba, J.H. Bowen, K. Nakayama, T. Kawahara, T. Sato, P. Richard, Y.-M. Xu, L.J. Li, G.H. Cao, Z.-A. Xu, H. Ding, T. Takahashi, Fermi surface nesting induced strong pairing in iron-based superconductors, Proc. Nation. Acad. Sci. (PNAS) 106 (18) (2009) 7330.
[4] M.R. Norman, Trend: high-temperature superconductivity in the iron pnictides, Physics 1 (2008) 21.
[5] H.-H. Wen, S. Li, Materials and novel superconductivity in iron pnictide superconductors, Annu. Rev. Condens. Matter Phys. 2 (2011) 121.
[6] S. Lee, J. Jiang, Y. Zhang, C.W. Bark, J.D. Weiss, C. Tarantini, C.T. Nelson, H.W. Jang, C.M. Folkman, S.H. Baek, A. Polyanskii, D. Abraimov, A. Yamamoto, J.W. Park, X.Q. Pan, E.E. Hellstrom, D.C. Larbelestier, C.B. Eom, The behavior of grain boundaries in the Fe-based superconductors, Nat. Mater. 9 (2010) 397.
[7] S. Lee, J. Jiang, J.D. Weiss, C.W. Bark, C. Tarantini, M.D. Biegalski, A. Polyanskii, Y. Zhang, C.T. Nelson, X.Q. Pan, E.E. Hellstrom, D.C. Larbalestier, C.B. Eom, Dependence of epitaxial $Ba(Fe_{1-x}co_x)_2As_2$ thin films properties on $srtio_3$ template thickness, IEEE Trans. Appl. Supercond. 21 (3) (2011) 2882.
[8] T.Y. Chen, Z. Tesanovic, R.H. Liu, X.H. Chen, C.L. Chien, A BCS-like gap in the superconductor $SmFeAso_{0.85}F_{0.15}$, Nature (London) 453 (2008) 1224.
[9] B. Gorshunov, D. Wu, A.A. Voronkov, P. Kallina, K. Iida, S. Haindl, F. Kurth, L. Schultz, B. Holzapfel, M. Dressel, Direct observation of the superconducting energy gap in the optical conductivity of the iron pnictide superconductor $Ba(Fe_0.9Co_0.1)_2As_2$, Phys. Rev. B 81 (2010) 060509(R).
[10] A. Perucchi, L. Baldassarre, S. Lupi, J.Y. Jaing, J.D. Weiss, E.E. Hellstrom, S. Lee, C.W. Bark, C.B. Eom, M. Putti, I. Pallecchi, C. Marini, P. Dore, Multi-gap superconductivity in a $BaFe_{1.84}Co_{0.16}As_2$ film from optical measurements at terahertz frequencies, Eur. Phys. J. B 77 (2010) 25–30.
[11] J. Yong, S. Lee, J. Jiang, C.W. Barj, J.D. Weiss, E.E. Hellstrom, D.C. Larbalestier, C.B. Eom, T.R. Lemberger, Superfluid density measurements of $Ba(Fe_{1-x}Co_x)_2As_2$ films near optimal doping, Phys. Rev. B 83 (2011) 104510.
[12] X. Zhang, Y.S. Oh, Y. Liu, L. Yan, S.R. Saha, N.P. Butch, K. Kirshenbaum, K.H. Kim, J. Paglione, R.L. Greene, I. Takeuchi, Evidence of a universal and isotropic $2\delta/K_BT_c$ ratio in 122-type iron pnictide superconductors over a wide doping range, Phys. Rew. B 82 (2010) 020515(R).
[13] R.T. Gordon, N. Ni, C. Martin, M.A. Tanatar, M.D. Vannette, H. Kim, G.D. Samolyuk, J. Schmalian, S. Nandi, A. Kreyssig, A.I. Goldman, J.Q. Yan, S.L. Bud'ko, P.C. Canfield, R. Prozorov, Unconventional london penetration depth in single-crystal $Ba(Fe_{1-x}Co_x)_2As_2$ superconductors, Phys. Rev. Lett. 102 (2009) 127004.
[14] B. Muschler, W. Prestel, R. Hackl, T.P. Devereaux, J.G. Analytis, J.-H. Chu, I.R. Fisher, Band- and Momentum-dependent Electron Dynamics in Superconducting $Ba(Fe_{1-x}Co_x)_2As_2$ as Seen via Electronic Ramman Scattering, Phys. Rev. B 80 (2009) 180510(R).
[15] C.W. Hicks, T.M. Lippman, M.E. Huber, J.G. Analytis, J.-H. Chu, A.S. Erickson, I.R. Fisher, K.A. Moler, Evidence for a nodal energy gap in the iron-pnictide superconductor LaFePO from penetration depth measurements by scanning SQUID susceptometry, Phys. Rev. Lett. 103 (2009) 127003.
[16] B. Kalisky, J.R. Kirtley, J.G. Analytis, J.-H. Chu, A. Vailionis, I.R. Fisher, K.A. Moler, Stripes of increased diamagnetic susceptibility in underdoped superconducting $Ba(Fe_{1-x}Co_x)_2As_2$ single crystals: evidence for an enhanced superfluid density at twin boundaries, Phys. Rev. B 81 (2010) 184513.
[17] J.H. Durrell, C.-B. Eom, E.E. Hellstrom, C. Tarantini, A. Yamamoto, D.C. Larbelestier, The behavior of grain boundaries in the Fe-based superconductors, Rep. Prog. Phys. 74 (2011) 124511.
[18] S. Lee, J. Jiang, J.D. Weiss, C.M. Folkman, C.W. Bark, C. Tarantini, A. Xu, D. Abraimov, A. Polyanskii, C.T. Nelson, Y. Zhang, S.H. Baek, H.W. Jang, A. Yamamoto, F. Kametani, X.Q. Pan, E.E. Hellstrom, A. Gurevich, C.B. Eom, D.C. Larbalestier, Weak-link behavior of grain boundaries in superconducting $Ba(Fe_{1-x}Co_x)_2As_2$ bicrystals, Appl. Phys. Lett. 95 (2009) 212505.
[19] C. Tarantini, S. Lee, Y. Zhang, J. Jiang, C.W. Bark, J.D. Weiss, A. Polyanskii, C.T. Nelson, H.W. Jang, C.M. Folkman, S.H. Baek, X.Q. Pan, A. Gurevich, E.E. Hellstrom, C.B. Eom, D.C. Larbalestier, Strong vortex pinning in Co-doped $BaFe_2As_2$ single crystal thin film, Appl. Phys. Lett. 96 (2010) 142510.
[20] Y. Zhang, C.T. Nelson, S. Lee, J. Jiang, C.W. Bark, J.D. Weiss, C. Tarantini, C.M. Folkman, S.-H. Baek, E.E. Hellstrom, D.C. Larbalestier, C.-B. Eom, X. Pan, Self-assembled oxide nanopillars in epitaxial $BaFe_2As_2$ thin films for vortex pinning, Appl. Phys. Lett. 98 (2011) 042509.
[21] S.M. Anlage, D.E. Steinhauer, B.J. Feenstra, C.P. Vlahacos, F.C. Wellstood, Near-field microwave microscopy of materials properties, in: H. Weinstock, M. Nisenoff (Eds.), Microwave Superconductivity, Kluwer, Amsterdam, 2001, pp. 239–269.
[22] S.M. Anlage, V.V. Talanov, A.R. Schwartz, Principles of Near-Field Microwave Microscopy in Scanning Probe Microscopy: Electrical and Electromechanical Phenomena at the Nanoscale, 1, Springer-Verlag, New York, 2007, pp. 215–253. ISBN: 978-0-387-28667-9)
[23] T. Tai, X.X. Xi, C.G. Zhuang, D.I. Mircea, S.M. Anlage, Nonlinear near-field microwave microscope for RF defect localization in superconductors, IEEE Trans. Appl. Supercond. 21 (2011) 2615.
[24] T. Tai, B.G. Ghamsari, T. Tan, C.G. Zhuang, X.X. Xi, S.M. Anlage, MgB_2 nonlinear properties investigated under localized high RF magnetic field excitation, Phys. Rev. ST Accel. Beams 15 (2012) 122002.
[25] T. Tai, B.G. Ghamsari, S.M. Anlage, I. Trans, Nanoscale electrodynamic response of Nb superconductors, Appl. Supercond. 23 (2013) 7100104.
[26] T. Tai, B.G. Ghamsari, S.M. Anlage, Modeling the nanoscale linear response of superconducting thin films measured by a scanning probe microwave microscope, J. Appl. Phys. 115 (2014) 203908.
[27] T. Tai, B.G. Ghamsari, T. Bieler, S.M. Anlage, Near-field microwave magnetic nanoscopy of superconducting radio frequency cavity materials, Appl. Phys. Lett. 104 (2014) 232603.
[28] T. Tai, Ph.D. dissertation, University of Maryland-College Park, 2013 Ph.D. thesis. See http://hdl.handle.net/1903/14668.
[29] T. Tai, B.G. Ghamsari, S.M. Anlage, Nanoscale electrodynamic vortex respose of nb superconductors, Precision Electromagnetic Measurements (CPEM), 2012 Conference on July (2012) 328–329.
[30] S.C. Lee, M. Sullivan, G.R. Ruchti, S.M. Anlage, Doping dependent nonlinear meissner effect and spontaneous currents in high-t_c superconductors, Phys. Rev. B 71 (2005) 014507.
[31] D.I. Mircea, H. Xu, S.M. Anlage, Phase-sensitive harmonic measurements of microwave nonlinearities in cuprate thin films, Phys. Rev. B 80 (2009) 144505.
[32] C. Jeffries, Q.H. Lam, Y. Kim, L.C. Bourne, A. Zettl, Symmetry breaking and nonlinear electrodynamics in the ceramic superconductor $YBa_2cu_3o_7$, Phys. Rev. B 37 (1988) 9840.
[33] S.C. Lee, S.Y. Lee, S.M. Anlage, Microwave nonlinearities of an isolated long $YBa_2Cu_3O_{7-\delta}$ bicrystal grain boundary, Phys. Rev. B 72 (2005) 024527.
[34] L. Ji, R.H. Sohn, G.C. Spalding, C.J. Lobb, M. Tinkham, Critical state model for harmonic generation in high-temperature superconductors, Phys. Rev. B 40 (1989) 10936–10945.
[35] A. Gurevich, G. Ciovati, Dynamics of vortex penetration, jumpwise instabilities, and nonlinear surface resistance of type-II superconductors in strong rf fields, Phys. Rev. B 77 (2008) 104501.
[36] M. Golosovsky, D. Davidov, E. Farber, T. Tsach, M. Schieber, Microwave transmission and harmonic generation in granular high-TC superconducting films: evidence for viscous flux motion and weak links, Phys. Rev. B 43 (1991) 10390.
[37] E.B. Sonin, A.K. Tagantsev, Vortex convection non-linearity of AC response of superconductors with weak links, Supercond. Sci. Tech. 4 (1991) 119–121.
[38] M.W. Coffey, Coupled nonlinear electrodynamics of type-II superconductors in the mixed state, Phys. Rev. B 46 (1992) 567–570.
[39] G.B. Lesovik, A.L. Fauchére, G. Blatter, Nonlinearity in normal-metal-superconductor transport: scatterring-matrix approach, Phys. Rev. B 55 (1997) 3146.
[40] A. Gurevich, V.M. Vinokur, Interband phase modes and nonequilibrium soliton structures in two-gap superconductors, Phys. Rev. Lett. 90 (2003) 047004.
[41] M. Putti, I. Pallecchi, E. Bellingeri, M.R. Cimberle, M. Tropeano, C. Ferdeghini, A. Palenzona, C. Tarantini, A. Yamamoto, J. Jiang, J. Jaroszynski, F. Kametani, D. Abraimov, A. Polyanskii, J.D. Weiss, E.E. Hellstrom, A. Gurevich, D.C. Larbalestier, R. Jin, B.C. Sales, A.S. Sefat, M.A. McGuire, D. Mandrus, P. Cheng, Y. Jia, H.H. Wen, S. Lee, C.B. Eom, New Fe-based superconductors: properties relevant for applications, Supercond. Sci. Technol. 23 (2010) 034003.
[42] C. Putzke, P. Walmsley, J.D. Fletcher, L. Malone, D. Vignolles, C. Proust, S. Badoux, P. See, H.E. Beere, D.A. Ritchie, S. Kasahara, Y. Mizukami, T. Shibauchi, Y. Matsuda, A. Carrington, Anomalous critical fields in quantum critical superconductors, Nat. Commun. 5 (2014) 5679.
[43] T. Tai, B.G. Ghamsari, T. Bieler, S.M. Anlage, Nanoscale nonlinear radio frequency properties of bulk Nb : origins of extrinsic nonlinear effects, Phys. Rev. B 92 (2015) 134513.